ACS Catalysis

Research Article

pubs.acs.org/acscatalysis

The Electronic Structure of [Mn(V)═O]: What is the Connection between Oxyl Radical Character, Physical Oxidation State, and Reactivity?

Daniel Charles Ashley[†] and Mu-Hyun Baik*[,‡,§]

[†]Department of Chemistry, Indiana University, 800 East Kirkwood Avenue, Bloomington, Indiana 47405, United States

[‡]Center for Catalytic Hydrocarbon Functionalizations, Institute for Basic Science (IBS), Daejeon 34141, South Korea

[§]Department of Chemistry, Korea Advanced Institute of Science and Technology (KAIST), Daejeon 34141, South Korea

Supporting Information

ABSTRACT: Mn^{V}═O functionalities are important in synthetic and bioinorganic chemistry, being relevant to both C−H activation and the O−O bond formation steps in enzymatic water oxidation, for example. The triplet and quintet spin states are believed to be active in these reactions, but they have only been sparingly characterized experimentally. Density functional theory (DFT) gives varying results, depending on the exchange-correlation functional employed, leading to ambiguity about whether the triplet Mn^{V}═O is better represented as Mn^{IV}−$O^{\bullet}$. While recent CASPT2 studies confirmed that the Mn^{IV}−$O^{\bullet}$ character is exaggerated by hybrid functionals, questions still remain about the nature of this bonding. Using high-level wave function methods, we investigated the fundamental relationship between the spin polarization, diradical character, and the physical oxidation state assignments. We conclude that, in terms of formal oxidation assignment, these species are best described as being between the Mn^{V}═O and Mn^{IV}−$O^{\bullet}$ extremes. While the extent of the oxyl radical character is exaggerated in B3LYP, it is significantly underestimated by local functionals. We also exploited the DFT-functional dependence of the oxyl radical character to examine its effect on O−O bond formation barrier heights and concluded that, although, for radical combination reactions, the oxyl character is a significant effect, for nucleophilic water attack reactions, the effect is much smaller and is likely not a requisite feature.

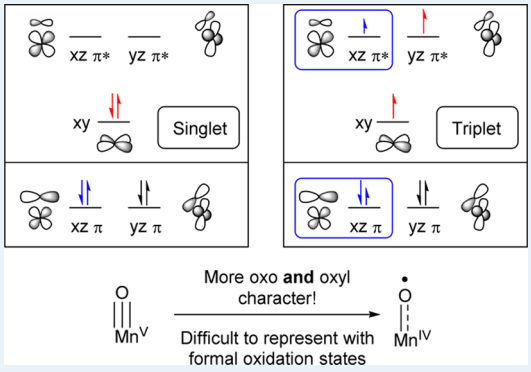

KEYWORDS: *water oxidation, C−H activation, manganese oxo, oxyl radical, DFT, CASSCF*

INTRODUCTION

Virtually every inorganic water oxidation catalyst features either a metal oxo or metal oxyl radical as a key species for generating dioxygen.[1−4] Among them are Fe,[5] Ru,[3] Co,[6] and Ir[7] complexes; yet, there are only few known Mn water oxidation catalysts, and they are generally less efficient.[8−13] The poor performance of Mn is disappointing from a biomimetic standpoint, as the only enzymatic, natural water oxidation catalyst in photosystem II (PSII),[14] which utilizes a Mn oxo cluster.[15,16] The high valent Mn^{V}═O moiety is key to catalytic reactivity and any deep mechanistic understanding must be built upon solid knowledge of its electronic structure. Previous density functional theory (DFT) work on the "blue dimer" established that Ru^{V}═O is better thought of as Ru^{IV} −$O^{\bullet}$.[1] Similar behavior was seen in numerous other systems, and it is now established that reactive M^{n}═O species are often better described as M^{n-1} oxyl radicals.[2] The concept that open-shell, radicaloid, electron-deficient, monoanionic oxyls are more reactive toward nucleophilic attack, radical coupling, and hydrogen atom transfer (HAT) reactions than closed-shell dianionic oxos makes sense intuitively. Siegbahn proposed[17] that the Mn^{V}═O species in the Brudvig catalyst[8] adopts the Mn^{IV}−$O^{\bullet}$ form, and that this formulation is required for facile O−O bond formation. The Mn^{V}═O and Mn^{IV}−$O^{\bullet}$ are resonance structures and, in reality, molecules adopt some combination of the two extremes (see Figure 1). In DFT studies with popular hybrid functionals, the Mn^{IV}−$O^{\bullet}$ form dominates the electronic structure typically. Many proposals exist for the critical O−O bond formation step in PSII, some invoking a nucleophilic attack on a Mn^{V}═O or Mn^{IV}−$O^{\bullet}$, implying Lewis acid/base behavior, while others explicitly rely on radical chemistry.[18]

Although DFT has been successful for certain types of metal oxos,[1] the Mn^{V}═O case is particularly challenging, as the extent of the redox noninnocence found can be heavily dependent on the DFT functional.[19,20] The triplet state of Mn^{V}═O shows the aforementioned oxyl radical character only when significant amounts of HF exchange are used.[21,22] Thus,

Received: June 25, 2016
Revised: September 7, 2016

DOI: 10.1021/acscatal.6b01793
ACS Catal. 2016, 6, 7202−7216

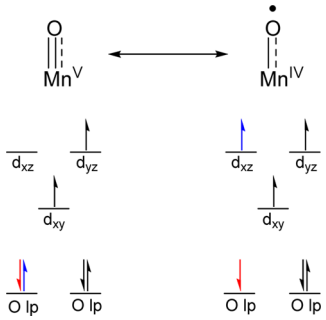

Figure 1. Resonance structures used for a simplistic description of triplet Mn^{V}=O.

the functional choice can skew which of the resonance structures in Figure 1 predominates. Since the diradical nature of Mn^{IV}–$O^{\bullet}$ is fundamentally multiconfigurational, it is more appropriate to use multireference methods such as Complete Active Space Self-Consistent Field theory (CASSCF). There has only been a few studies addressing how much HF exchange is needed to accurately match multireference calculations in this respect for other systems.[19,20] Irrespective of these complications, the research community relies on DFT methods to describe reaction intermediates, where there are often very little experimental data available. The fact that different exchange-correlation functionals can give qualitatively different electronic structures is a serious problem, and was recently investigated for Mn^{V}=O porphyrin complexes by Pierloot, where it was concluded that B3LYP and other hybrid functionals exaggerate the oxyl radical character greatly, when compared to CASPT2 results.[23] Numerous groups have extensively studied the reactivity and electronic structure of high-valent manganese oxos.[24−33] Yet, while much is known, the presence or absence of radical character and the role it may play in reactivity is still unknown, and it remains a subject of ongoing debate.[34]

Here, we employed several chemically relevant, six-coordinate model systems of Mn^{V}=O, shown in Chart 1.

Chart 1. Models Used in This Study

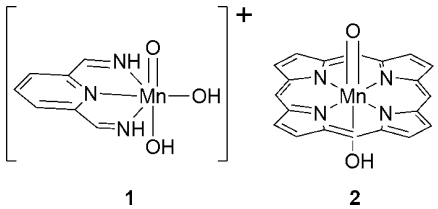

1 2

The focus of this work was to explore the chemical meaning of the magnitude of oxyl radical character, in terms of fundamental electronic structure and reactivity. To this end, we used CASSCF and multireference perturbation theory to scrutinize the relationships between radical character and spin state to physical oxidation states, and how these are all connected to our formal oxidation-state assignments. Finally, we investigated the impact of the DFT-dependent oxyl radical character on calculating barrier heights for prototypical O–O bond formation reactions. All of these issues are fundamental concepts in physical inorganic chemistry that are commonly invoked in interpretation of experimental results. Indeed, one of the great benefits of computational chemistry to the experimental community is its ability to provide information on the qualitative and quantitative validity of electronic structure assignments of fleeting or otherwise inscrutable species. Thus, these are far from being minor methodological issues, but rather problems that can dramatically affect our formulation of reactive intermediates in mechanism formulation and structure analysis.

COMPUTATIONAL DETAILS

DFT, CASSCF, and N-Electron Valence Perturbation Theory (NEVPT2)[21] calculations were performed with Orca 3.0.[35] DFT geometry optimizations were carried out using the B3LYP[36−40] functional and the 6-31G** basis set.[41] Manganese was represented by the LANL2DZ basis, including an effective core potential (ECP).[42] The energies and population analyses were refined by performing single-point energy calculations on the optimized structures using the all-electron cc-pVTZ basis set on all atoms.[43,44] All DFT-optimized structures were confirmed to be minima by performing vibrational frequency calculations to verify that there were no imaginary modes. For studies on reactivity, the Jaguar 8.1[45] program was employed, primarily because we have extensive experience in modeling transition states and mechanisms with Jaguar. The same basis sets were employed here for the geometry optimizations. Single-point energies were calculated using cc-pVTZ(-f) on all light atoms, while Mn was represented using LACV3P, which is a modified version of LACVP, where the exponents have been decontracted to match the ECPs with triple-ζ quality. No significant differences were found between the different programs/methodologies. Analytical vibrational frequencies were calculated within the harmonic approximation at the double-ζ level to ensure that all structures reported were well-defined minima with no imaginary frequencies.

To examine the impact of using various amounts of Hartree–Fock exchange, modified forms of B3LYP were used where the parameter a in eq 1 was varied. Parameters b and c were left fixed at 0.72 and 0.81, respectively. The resultant functionals were referred to as B3LYP[X], where "X" is the value of a, expressed as a percentage.

$$\mathrm{B3LYP} = (1-a)E_x^{\mathrm{LDA}} + aE_x^{\mathrm{HF}} + b\Delta E_x^{\mathrm{B}} + (1-c)E_c^{\mathrm{LDA}} + cE_c^{\mathrm{LYP}} \quad (1)$$

Optimized CASSCF wave functions were used as reference states for NEVPT2 calculations to account for dynamic correlation effects. All CASSCF/NEVPT2 results were calculated using cc-pVTZ on all atoms. The choice of the active space (AS) is the most critical decision in any CASSCF study. A general series of rules for how to choose an appropriate AS for a transition-metal complex has been established elsewhere[46,47] and was generally followed here. All five d-orbitals were included, four of which were antibonding, in addition to the four bonding combinations with ligand-based orbitals that will be present for a pseudo-octahedral metal oxo. The d(xy)-orbital was considered nonbonding. Therefore, the minimal AS was 10 electrons distributed in 9 orbitals (10,9). We were not interested in investigating the additional complication of the redox-activity of the porphyrin in **2**, resulting in the omission of porphyrin-based orbitals from our active space, which admittedly is not typical for CASSCF studies of metalloporphyrins complexes. Given that we only investigated states where the porphyrin is expected to be redox-inactive (*vide infra*), we felt that this was an acceptable deficiency in our method. This is further validated by reasonable qualitative agreement of our results on the oxyl

DOI: 10.1021/acscatal.6b01793
ACS Catal. 2016, 6, 7202–7216

radical character and electronic distribution of **2** with CASPT2 studies of other porphyrinoid complexes.[23,48]

For some systems, a second set of d-orbitals ("double shell") is necessary. We found that the inclusion of various double shells had a minimal effect on the radical character on the oxo, so we only extensively discuss the results with the (10,9) AS. For **1**, there is significant α spin on the *cis*-hydroxide ligands and, to a lesser extent, the *trans*-hydroxide ligands, which, in part, prompted us to design active spaces where hydroxide π-interactions were included. In all active spaces examined, the spin on the *trans*-hydroxide was negligible, but the spin on the *cis*-hydroxide was significant in some active spaces. Although the expanded active spaces occasionally induce minor changes in the spin or bond length, they were never enough to change our general conclusions. Results for all expanded active spaces including double shells are discussed further in the Supporting Information.

A typical approach when employing high-level *ab initio* calculations is to use a judiciously chosen DFT method to generate optimized structures, and then apply higher-level single-point calculations. This operates on the assumption that CASSCF is not needed to accurately describe the geometry, which is a reasonable assumption in many, but not all,[49] cases, but given that the functional choice has a strong impact on the Mn−O bond length, because of the extent of diradical character, a different method for determining the structure had to be employed. Since the multiconfigurational behavior is largely confined to the Mn−O bond, both in chemical reality and by virtue of the AS used, only this one bond length needs to be optimized at the multiconfigurational level, and the structure of the rest of the molecule can be assumed to be relatively invariant to the functional choice. In reality, different functionals can and do sometimes provide differences in other structural parameters; however, presently, these were not of any serious interest to us, so we have taken the B3LYP structural results to be reasonable. Fully optimized structures were generated by performing a relaxed scan along the Mn−O distance using B3LYP, followed by CASSCF/NEVPT2 calculations performed at each point. The net result is a curve showing where the NEVPT2 energy is minimized as a function of the Mn−O distance, thus enabling the calculation of a consistent Mn−O bond length. Note that the reported values were determined with NEVPT2 at the triple-ζ level, while the DFT structures were determined at the double-ζ level. To ensure that the structural differences between NEVPT2 and DFT reflect on method, and not simply the size of the basis set, relaxed scans with B3LYP and B3LYP[0] were performed at the triple-ζ level in a manner analogous to that of the NEVPT2 scans. Generally, similar results were obtained, and these are thoroughly discussed in the Supporting Information. Finally, our goal was not to obtain accurate spin-state energies, since it was not directly related to the questions at hand, and has already been extensively explored elsewhere.[23,50] However, we briefly discuss the quality of our spin-state energetics in the Supporting Information.

RESULTS AND DISCUSSION

Spin States and Molecular Orbital (MO) Diagrams. The most important spin states for Mn^{V}=O complexes are singlet, triplet, and quintet states. Conceptual molecular orbital (MO) diagrams for the singlet and triplet states in pseudo-octahedral structure are shown in Figure 2. The oxo ligand is a strong σ- and π-donor, and the ordering of the d($x^2 - y^2$) and d(z^2) is dependent on whether the oxo is a stronger σ-donor than the equatorial ligands present in the particular complex. Generally, π-donation increases the energy of the d(xz) and d(yz)-orbitals in the frontier orbital space, since their character is M-oxo antibonding. As illustrated in Figure 2, the singlet state has a pair of electrons in the d(xy)-orbital. In the triplet state, one of these electrons can be thought of having been flipped and placed in the d(yz)-orbital. The quintet state represents the high-spin state of the Mn complex with the nonbonding d(xy) and both π*-orbitals, d(xz) and d(yz), occupied by one unpaired electron each. In addition, the π-orbital d(xz) is also half-filled, as illustrated in Figure 2.

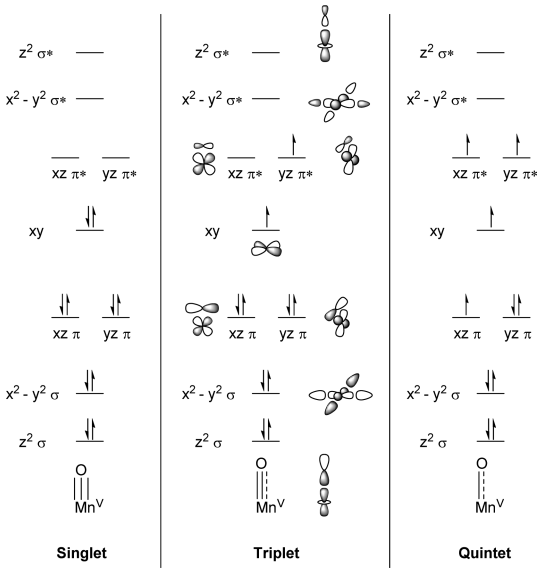

Figure 2. Simplified MO diagrams for all considered spin states of Mn^{V}=O in a pseudo-octahedral environment. These MO diagrams represent the (10,9) active space used in this work.

In many water oxidation catalysts, the Mn^{V}=O functionality adopts a triplet ground state,[17,51,52] whereas, in most porphyrinoid complexes of Mn^{V}=O, the ground state is a closed-shell singlet,[23,53,54] in which the oxygen has no radical character whatsoever. The triplet and quintet states are thought to become preferred at the transition state, and may be important for understanding the chemical reactivity displayed by these molecules.[55,56] Despite the popularity of this argument, a recent combined experimental and computational study demonstrated that sulfoxidation by a high-valency Mn^{V} oxo complex proceeds through the singlet state and does not cross to the triplet surface.[50] Higher spin states can show significant spin density on oxygen and are characterized by elongated Mn−O bonds, reflecting on the increased population of metal−oxygen π*-orbitals. Our model complex **1** carries a pyridine(diimine) (PDI) ligand and two hydroxides coordinated to Mn, as shown in Chart 1. This minimalistic model captures key elements of the electronic structure found in metal-polypyridyl fragments that are found in many synthetic water oxidation catalysts, and the hydroxides mimic the oxo/hydroxo bridges found, for example, in the natural oxygen-evolving complex (OEC) of photosystem II.[14,15] However, model **1** is not a good model for porphyrinoid complexes; therefore, model **2**, which contains a full porphyrin ligand and an axial hydroxide, *trans* to the oxo, was also included. Groves has studied the reactivity of similar complexes,[53,54,57,58] and **2** itself has been analyzed with DFT previously.[55] Each model is

DOI: 10.1021/acscatal.6b01793
ACS Catal. 2016, 6, 7202−7216

treated both as a singlet and a triplet, and the quintet state is considered for **1**. Quintet states for **2** are not studied, because it has been established that, for Mn^{V}=O porphyrinoids, these involve electron transfer from the porphyrin to the metal to form "Compound I" type systems.[48] While this is an important electronic feature, the focus of the present work was on the Mn^{V}=O functionality without the complicating redox activity of the porphyrin (see the section entitled "Computational Details").

For **1**, we found only one meaningful structural conformer for the singlet, but the triplet and quintet show several conformers, as shown in Figure 3 (denoted as $\mathbf{1}_a$ and $\mathbf{1}_b$).

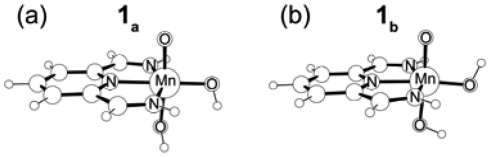

Figure 3. B3LYP optimized structures of (a) triplet $\mathbf{1}_a$ and (b) triplet $\mathbf{1}_b$.

Electronically, $\mathbf{1}_b$ is lower in energy by ∼4 kcal/mol at the B3LYP level, but both conformers are important to consider: When **1** is engaged by a water molecule in a nucleophilic attack, conformer $\mathbf{1}_a$ will be relevant, as the *cis*-hydroxo group can deprotonate the nucleophilic water only in this structural arrangement. Because $\mathbf{1}_a$ has a larger dipole moment, it exhibits a greater solvation energy by ∼3 kcal/mol and the two conformations become isoenergetic in water. Closer examination of $\mathbf{1}_a$ and $\mathbf{1}_b$ show that they correspond to slightly different electronic states. This is a relatively minor point, but is thoroughly discussed in the Supporting Information.

Table 1 summarizes the calculated Mn−O bond lengths and spin populations on the oxo determined by CASSCF/NEVPT2, B3LYP, and B3LYP[0].[59] Generally, B3LYP significantly overestimates the oxyl radical character, while B3LYP[0] underestimates it, compared to CASSCF results. For instance, B3LYP[0] predicts a Mn−O bond length of 1.63 Å and a Mulliken spin on the oxo of 0.21 for $\mathbf{1}_a$, whereas B3LYP gives values of 1.72 Å and −0.73, respectively. Here, positive numbers indicate an excess of α electrons, whereas the overpopulation of β electron density is shown using negative numbers. As illustrated in Table 1, the values determined with CASSCF/NEVPT2 fall between these values with a Mn−O bond length of 1.66 Å and a Mulliken spin of −0.22, suggesting that the Mn−O bond is best characterized as having intermediate diradical character, which is a result that is consistent with other CASSCF studies.[23,50]

Table 1. Key Triplet Parameters Determined Using CASSCF/NEVPT2 (Referenced as CASSCF in the Table), B3LYP, and B3LYP[0]

methodology	*d*(Mn−O) (Å)	Mulliken Spin on oxo	Mulliken Spin on Mn	Mulliken Spin on *cis* OH	Mulliken Spin on *trans* OH
Model $\mathbf{1}_a$					
B3LYP	1.72	−0.73	2.59	0.13	0.08
B3LYP[0]	1.63	0.21	1.56	0.24	−0.04
CASSCF	1.66	−0.22	2.32	−0.12	0.01
Model $\mathbf{1}_b$					
B3LYP	1.75	−0.79	2.60	0.12	0.14
B3LYP[0]	1.64	0.20	1.59	0.23	−0.08
CASSCF	1.67	−0.29	2.37	−0.10	0.01
Model 2					
B3LYP	1.75	−0.81	2.91		0.12
B3LYP[0]	1.64	0.17	1.81		−0.06
CASSCF	1.69	−0.29	2.35		0.01

[a]All reported spins were obtained from single-point energy calculations employing cc-pVTZ on all atoms.

Figure 4 shows how the bond length and Mulliken spin density change as the amount of HF exchange is varied. In addition, the DFT orbitals were recast as natural orbitals and the natural orbital occupation numbers (NOONs) of the "empty" π^*-orbital where oxyl radical character can develop were plotted in Figure 4. Comparing Figures 4a and 4b with the CASSCF values calculated in Table 1, it can be seen that there is no one degree of HF exchange that matches the CASSCF/NEVPT2 results reliably for all systems. $\mathbf{1}_a$ treated with 13%−14% HF exchange gives the best match for spin and bond length; however, for $\mathbf{1}_b$, a B3LYP version with 12% HF exchange affords reasonable agreement with the CASSCF values. Finally, the oxyl spin of **2** agreed with CASSCF with

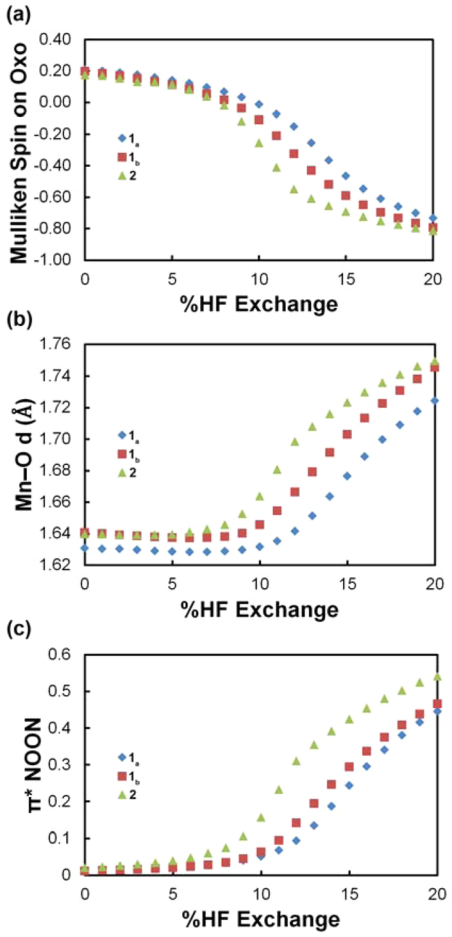

Figure 4. Dependence of features related to oxyl radical character on the amount of HF exchange included in the functional: (a) Mulliken spin population on the oxo oxygen, (b) Mn−O bond length, and (c) NOON of the M−O π^*-orbital where diradical character originates. Legend for all panels: blue diamonds, $\mathbf{1}_a$; red squares, $\mathbf{1}_b$; and green triangles, **2**.

DOI: 10.1021/acscatal.6b01793
ACS Catal. 2016, 6, 7202−7216

~10% HF exchange, whereas the bond length was more accurately calculated with 11%−12%. Overall, a range of HF exchange from ~10%−14% was necessary for BS-DFT to produce acceptable agreement with the MCSCF calculations. Intermediate values for HF exchange have been proposed as being more accurate for spin-state energetics as well; when combined with our results, it suggests that these intermediate values may be more accurate for both energetics and spin density.[60] Generally, our results suggest that pure functionals and those with more than 15% HF exchange should be used with caution for diagnosing oxyl radical character. While our conclusions agree with other studies in that large amounts of HF exchange should be avoided,[23,50] calculations on our models also show that pure functionals are inappropriate as well. Clearly, accurate functional benchmarking must be considered over a wide range of structures and models, especially given that the exact geometry of the OEC at the S_4 state is not known.[14,18,61]

The better agreement obtained using DFT functionals with intermediate amounts of HF exchange compared to CASSCF/NEVPT2 values is an important result, because pure functionals and functionals with more than 15% HF have been used extensively in the past in similar systems. For example, B3LYP was used by Siegbahn to demonstrate dramatic oxyl radical character,[17] while Crabtree et al. used BP86, which gave rise to their conclusion that there was only very small oxyl radical character.[55] Notably, in some of Siegbahn's work, B3LYP*[62,63] has been employed and results similar to those of B3LYP were observed. Of course, the exact functional dependence will be dependent on the specific system, as is demonstrated here.

Interestingly, the B3LYP[0] results do not agree with the CASSCF conclusions, even though the computed absolute amount of spin on the oxo moiety is similar to that calculated with CASSCF, 0.21 and −0.22 respectively, for $\mathbf{1}_a$. When the Mulliken population analysis reveals a relatively high positive or negative number, it is fairly safe to assume that the respective unpaired electron cloud is present in excess at that atom. If a small number is obtained, it is tempting to conclude that there is no unpaired electron density present at the particular atom. This view can be highly misleading in open-shell electronic structures. A small overall Mulliken population value can be either the result of all electrons being paired in a closed-shell sense, or also when there is an equal amount of unpaired α and β electron densities in orthogonal orbital subspaces. This is important, because unpaired electrons on the oxygen has been widely recognized as key for chemical reactivity and relatively large Mulliken spin populations were taken as an indicator of such situation.[1] In complex open-shell configurations, a small Mulliken spin population value does not necessarily indicate an electronic structure that resembles a closed shell.

B3LYP[0] predicts roughly two unpaired α electrons on the metal, and a small amount of residual α spin is delocalized onto the oxo ligand. Such a small amount of α spin on the oxygen is indicative of the d(xz) and d(yz)-orbitals being not purely metal based, but are Mn-oxo π*-orbitals that contain a small amount of oxygen character, as illustrated in Figure 2. Small amounts of spin delocalization onto ligands are typical for transition-metal complexes; this is a point that has been well-argued previously by McGrady,[21] with respect to Crabtree's study.[55] It is intriguing that, despite having such low diradical character, these complexes were capable of C−H activation, challenging the paradigm that radical character is required for reactivity. The fact that some α spin delocalizes on to the oxygen highlights the fact that the Mulliken spin on the oxygen will reflect both the β spin in the d(xz)-orbital, as shown in Figure 2, and the α spin from the d(yz)-orbital, as discussed earlier. A total spin of zero on oxygen, which occurs at ~10% and ~8% HF exchange for **1** and **2**, respectively, means that the β spin is cancelled by an equal amount of α spin in a different orbital. Thus, the oxygen radical character in the xz-space will be underestimated when only the overall Mulliken spin is considered. However, this effect is not large, as evidenced by the fact that the residual α spin is only ~0.2 when no HF exchange is employed, which is consistent with previously reported results.[23] Regardless, a complete lack of diradical character in the xz-space should be associated with an overall oxo Mulliken spin of ~0.2, not 0. The existence of α spin in one π-space and β spin in another was examined by Pierloot,[23] where it was suggested that these spin differences may result in different types of reaction being mediated by the same bond. We present a similar argument, with respect to acidity/basicity below. As intriguing as this proposal may be, we must be careful not to overinterpret this very small amount of α spin, as it may be construed as spin-bleeding as discussed above.

Generally, the spin densities track well with a less ambiguous metric: the Mn−O bond length. Given the correlation with the Mulliken spin, NOONs, and the MO arguments presented above, it is clear that the Mn−O bond length is strongly associated with the radical character in the xz-orbital space. This can be seen in Figure 4b, where changes in bond length can be seen up to ~8% HF exchange. At approximately the same %HF, the changes in NOONs and Mulliken spin cease with the spin on oxygen being ~0−0.1, which suggests that while the residual α spin should not be ignored, the primary factor in the variations of the Mn−O bond length should be the diradical character in the xz-space. The dominance of the diradical character in the xz-space is indicated by the functional dependence of the NOON for the d(xz)-orbital, which is consistent with the changes in bond length and spin.

It is convenient to quantify the diradical character using NOONs via eqs 2 and 3.

$$b_i = \frac{n^+ - n^-}{2} \tag{2}$$

$$y = 1 - b_i \tag{3}$$

Equation 2 shows the calculation of the effective bond order (b_i), as a function of the NOON of the bonding (n^+) and antibonding (n^-)-orbitals. The diradical character is mostly localized in a single pair of π bonding and antibonding orbitals (*vide infra*), and these are the orbitals that we use for these calculations. From b_i, the diradical character y can be calculated. For BS-DFT spin, contamination can lead to an overestimation of diradical character. Therefore, an alternative method of calculating diradical character that explicitly only takes into account the weight of double excitations has been used[20,64] and is shown in eq 4:

$$y_{corr} = 1 - \frac{2b_i}{1 + b_i^2} \tag{4}$$

Note that there are other similar ways to conduct such analyses, as has been done by Shaik and co-workers.[65−67]

Table 2 summarizes the calculated diradical characters for triplets $\mathbf{1}_a$, $\mathbf{1}_b$, and **2**. Using B3LYP, the value of the parameter y is calculated to be 0.45, indicating that $\mathbf{1}_a$ can be considered to

DOI: 10.1021/acscatal.6b01793
ACS Catal. 2016, 6, 7202−7216

Table 2. Calculated Diradical Character of Triplets Determined Using CASSCF/NEVPT2 and DFT

methodology	n^+	n^-	y	y_{corr}
		Model 1_a		
B3LYP	1.55	0.45	0.45	0.15
B3LYP[0]	1.99	0.01	0.01	0.00
CASSCF	1.65	0.36	0.36	
		Model 1_b		
B3LYP	1.53	0.47	0.47	0.17
B3LYP[0]	1.99	0.01	0.01	0.00
CASSCF	1.62	0.38	0.38	
		Model 2		
B3LYP	1.46	0.54	0.54	0.24
B3LYP[0]	1.98	0.02	0.02	0.00
CASSCF	1.58	0.42	0.42	

[a]All NOONs were obtained from single-point energy calculations employing cc-pVTZ on all atoms. y_{corr} was only calculated for DFT results.

have a diradical character of 45%. However, B3LYP[0] predicts that there is only negligible diradical character with the value of y being only 0.01: that is, a predicted diradical character of merely 1%. The CASSCF calculation is in reasonably good agreement with the B3LYP results and a diradical character of 36% is calculated. The largest diradical character calculated with any method or complex is 54% for **2** with B3LYP, which is in reasonable agreement with DFT results previously reported by Yamaguchi on Mn^V=O oxo complexes, where the formal diradical character was found to be under ~50%,[68−70] based on y_{corr} values. Typically, the y_{corr} parameters are significantly smaller than y. For example, 45% radical character was calculated for $\mathbf{1}_a$ with B3LYP, but the corresponding y_{corr} value is 15%. Using y_{corr}, we conclude that the removal of spin contamination in the B3LYP results gives *less* diradical character than the CASSCF results, which is a conclusion that was also reached for copper corroles.[20]

Spin contamination in BS-DFT has been heavily studied;[71] however, generally, it is not always clear how to compare spin contaminations in DFT to that in HF-based wave functions. However, it is well established that BS-DFT wave functions must have spin contamination present, as it is essential to how they are constructed as mixtures with higher lying spin states.[72] Although some of the properties of these BS-wave functions are unphysical, they can provide a realistic density of a multiconfigurational system, assuming that the chosen functional is appropriate for a given system.[73] That being said, generally, no form of BS-DFT has been parametrized to consistently and accurately describe diradical character effectively;[71] therefore, it is not clear how much spin contamination should be corrected *a priori*. An additional point is that, assuming that BS-DFT spin contamination should be treated similarly to HF, there would still be reason to not project out all single excitation character from our wave functions. Equation 4 only includes double excitations as part of the diradical character. As shown by Rowland,[74] single excitations can be relevant in the ground-state wave function if the local electronic environments of the orbitals involved differ, as in our case, where the diradical electrons are shared between two different elements. In fact, our CASSCF results show that single excitations are just as important as the double excitations (*vide infra*). All these points taken together suggest that, while y is overestimating the diradical character due to excessive spin contamination, y_{corr} is most likely underestimating it by neglecting the importance of single excitations, and the fact that some spin contamination is likely intrinsic to a correct BS-DFT wave function. Therefore, it is encouraging that our CASSCF diradical characters lie between these two extremes, suggesting that these wave functions are incorporating a reasonable amount of diradical character, and can be used as a point of reference for calibrating BS-DFT wave functions.

Based on the Mulliken spins and Mn−O bond lengths obtained with CASSCF/NEVPT2, it is clear that there is less radical character on oxygen than commonly assumed for a genuine "oxyl radical". Siegbahn has previously described a system, which was known to be inactive toward water oxidation, with a spin of −0.23 on oxygen as being "mainly a Mn^V-oxo state".[17] However, it is equally important to recognize that these systems display significantly more radical character than that expected for a genuine "closed shell" oxo. When the Mulliken spin, bond length, and diradical character are all taken together, it can be seen that they all fall between the values predicted by B3LYP and B3LYP[0]. The most reasonable conclusion is simply that the Mn^V=O bond is poorly described by either extreme and is best considered to exist somewhere intermediate on the continuum of radical behavior. Finally, it is important to note that, although they are not nearly as dramatic, there are some DFT functional dependencies exhibited by the singlet and quintet states. These are discussed in detail in the Supporting Information.

The Relationship between Radical Character, Spin State, and Physical Oxidation State. While Mulliken spin analysis and radical character are interesting in their own right, they serve a critical diagnostic role in the assignment of oxidation states. While analyzing these issues of how accurate the "radical" descriptor of these electronic structures were, we became interested in understanding how realistic is it to invoke a change in physical oxidation state upon going from the singlet to the higher lying spin states. Note, we are not interested in assigning "absolute" oxidation states, because those are more or less arbitrary. Rather, we wish to understand if the picture so often invoked of the singlet represented as Mn^V=O and the triplet and quintet being represented as $Mn^{IV}-O^{\bullet}$ meant that there were genuine changes in the electron density around Mn and O associated with changing spin state. If the electron density changes as expected, the oxygen atom in the triplet and quintet states should become more electron-deficient, in comparison to the singlet states, and *vice versa* for the metal. It is important to understand changes in physical oxidation state, as they can have a large impact on the role of electrostatic interactions in chemical reactivity. Groves reported previously that the triplet and quintet states of a Mn^V=O porphyrin had more electron-rich oxos than the singlet states based on charge analysis and solvation energies,[53] which runs counter to the expectation based on the increasing oxyl radical character of these spin states. Similarly, a recent DFT study by Kim on Fe^{IV}=O-based C−H activation, which is believed to become $Fe^{III}-O^{\bullet}$ as the Fe−O bond is elongated, found that, along the reaction coordinate, the α electrons transferred from oxygen to Fe were comparable if not slightly less than the β electrons transferred from Fe to O.[75] These counterintuitive physical oxidation state changes were not explained in detail in either of these cases. In contrast to these examples, DFT analysis of a Mn^{IV}=O/$Mn^{III}-O^{\bullet}$ system found that, even though the $Mn^{III}-O^{\bullet}$ resonance structure assignment was more consistent with the experimental results, hydrogen-bond donors would

DOI: 10.1021/acscatal.6b01793
ACS Catal. 2016, 6, 7202−7216

cause it to collapse back to the Mn^{IV}=O state, suggesting that this system possessed a more electron-rich oxo, as would be predicted from the formal oxidation-state assignments. The high-level calculations performed here afford the opportunity to carefully explore the relationship between spin, diradical character, and physical oxidation state beyond the innate uncertainties associated with density functional methods. Characterization of these qualities is tractable by carefully using population analysis methods, of which there are many different types, and we found it useful to use natural orbital composition and NOONs to track the electron distribution (*vide infra*).

Figure 5 shows MO diagrams illustrating the effect of a double excitation from a metal−ligand π-bonding MO to its

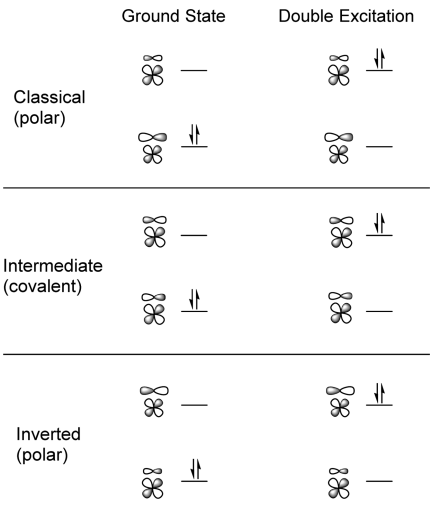

Figure 5. Depiction of how charge-transfer excitations are related to bond composition.

antibonding π* counterpart. Diradical character is related to the extent of which double and single excitation configuration state functions (CSFs) are included in the multiconfigurational wave function. Different types of diradicals can involve different types of dominant excitations.[74] Given the multideterminantal nature of the single excitations, they are more difficult to show diagrammatically and, therefore, only the double excitations are shown. Three scenarios are possible:

(1) First is the *classical* case, where the bonding orbital is ligand-based and the antibonding orbital is metal-based, which is the typical behavior for metal complexes where the ligands are "redox-innocent".
(2) Next is the "*inverted*" case,[21,76] where the bonding orbital is metal-based, and the antibonding orbital is ligand-based.
(3) Finally, the case of a *perfectly covalent* bond is shown, where the bonding and antibonding orbitals have the same amount of ligand and metal character.

For the classical case, the double excitation will cause significant charge transfer from the ligand to the metal, leading to a change in physical oxidation state (specifically, a removal of electron density from the ligand). In the inverted case, excitation will cause charge-transfer from the metal to the ligand. In the covalent case, excitation will not induce charge transfer and, hence, does not change the physical oxidation state of the atoms involved. To quantify which of these descriptions is most applicable, we calculated the degree of covalency (DC), as shown in eq 5.

$$\mathrm{DC} = \frac{C_a}{C_b} \tag{5}$$

Here, C_a and C_b refer to the percent composition of the antibonding and bonding MOs, respectively, in terms of the ligand's contributing basis functions.

Generally, covalent bonds should show more multiconfigurational character[77] than polar bonds in this context.[47] However, this does not mean that polar bonds will not show any multiconfigurational character or that all covalent bonds will be multiconfigurational. To more reliably quantify and analyze the physical oxidation state, as a function of these interactions that are potentially accompanied by charge transfer, both the orbital composition, which will show qualitatively the covalent/polar character of the bond, and the NOON, which will reflect the weight of both single and double excitations, must be considered. In reality, orbital composition and NOONs are not so neatly separable, but given that NOONs are such a clear quantifier of multiconfigurational character, we feel that the above simplification is conceptually useful. We related these concepts to each other by defining an "effective electron count" (EEC), as shown in eq 6:

$$\mathrm{EEC} = \sum_n (O_n \times C_n) \tag{6}$$

The EEC will represent the amount of electrons that effectively belong to an atom over n molecular orbitals. Here, O_n and C_n are the occupation number of the nth MO and percent composition of the nth MO, in terms of the atom's contributing basis functions.[78] The EEC can be expressed considering all of an atom's particular basis functions, which will reflect the total number of electrons taken to belong to the atom. What is more useful in terms of carefully dissecting the electronic structure is to calculate the EECs using only particular basis functions for an atom over a specific set of MOs, which can be used to analyze, bond by bond, how the electron density is distributed in these complex systems. We focused on calculating EECs using the p-orbitals on oxygen, but defined them in terms of the relevant M−O bonds. For example, calculating the EEC on oxygen in the "π_{xz}-space" would inform us regarding how much electron density was localized on oxygen as a result of the π and π* interactions with the d(xz)-orbital. When the molecule is perfectly symmetric, this simply involves using eq 6 with only O p_x-orbitals, but any distortions to lower symmetry can give rise to mixing of other p-orbitals into this MO. Generally, we use all of the O p-orbitals, but make purposeful choices with regard to what MOs to include in our set. For example, in the calculation of EEC_{xz}, we included the MOs that are clearly well-described as interactions with d(xz).

As is the case with all population analyses, many other approaches can be imagined, but the EEC method is attractive, because of its simplicity and straightforward connection to the natural orbital composition, thus, making the decision about the diradical character intuitive and consistent across different species. We begin the analysis with the singlet state, since it is considered to be well-represented as a closed-shell Mn(V) triply bonded to an oxo ligand, or at least significantly more so than the higher spin states, where Mn is considered to have acquired more Mn(IV) character, and the O atom more oxyl radical character. Importantly, the singlet state is usually not

DOI: 10.1021/acscatal.6b01793
ACS Catal. 2016, 6, 7202−7216

considered to be the reactive spin state for C−H activation or water oxidation, and oxyl radical character may be the key difference. Assuming the reasonable hypothesis that the singlet has small or no oxyl radical character is correct, there should be a significant difference in physical oxidation state between the singlet and triplet cases. Note that we will formally refer to the singlet states as a "Mn(V)−oxo(−II)", but not in a literal or absolute sense. We are only interested in how the physical oxidation state *changes* as a function of spin state and developing diradical character.

The active space for the calculation of singlet **1** is shown in Figure 6. The natural orbitals show that each Mn−O bond has

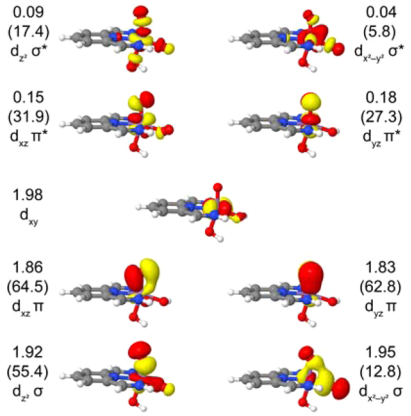

Figure 6. Natural orbitals (iso values: 0.05 a.u.) and NOONS for singlet **1**. The percentage of oxygen character of each MO, if it was significant, is listed in parentheses.

its bonding orbital polarized toward oxygen, and its antibonding orbital polarized toward the metal; i.e., it can be described as "classical", supported by the DC values of 0.49 and 0.43 for the π_{xz} and π_{yz} spaces, respectively. Note that the optimized structures of singlet **1** and **2** do not have linear O−Mn−OH angles. Instead, they are slightly bent to 162.8° and 164.9°, respectively, likely because of the stronger *trans*-influence of the oxo group. The distorted geometry causes the π_{xz}-space to be skewed. NOONs of the Mn−O π^*-orbitals, are 0.15 and 0.18, indicating that there is some radical character in these bonds. For a useful point of comparison, a CASSCF calculation on the π system of ethylene (2,2) at the same level of theory yields NOONs of 1.92 and 0.08 for the π- and π^*-orbitals, which, although smaller than those seen in singlet **1**, are comparable. Describing ethylene as having significant radical character would be misleading, since it is dominated by a single CSF at ∼95%. Therefore, although these levels of excitation in the individual π-bonds of singlet **1** are indicative of multiconfigurational character, it should not be taken as an example of high diradical character per bond. However, the composition and occupation of each M−O π^*-orbital is essentially identical, meaning that the sum of the diradical character in both of these bonds becomes more substantial and is comparable to the triplet (*vide infra*). Analysis of the multiconfigurational wave function in terms of the weights of the CSFs reveal that it is mostly dominated by the CSF shown in Figure 2 (79.5%) and single (3.3% for simultaneous single excitation in each bond) and double excitations (3.8% and 2.3% for each π-bond) within the π-space comprise the other dominant CSFs. A CASSCF wave function is considered more single-configurational the larger the contribution is from the dominant state. Although there is no absolute cutoff for how much the wave function should be dominated by a single CSF, we may consider ∼80% to still be significantly multiconfigurational.[49] The ∼80% value reported here agrees well with a previous study on a singlet Mn^{V}=O salen complex.[79] A final note about the orbital analysis that is relevant for all spin states is that the metal orbitals involved with σ-bonding with the oxo and the other ligands often mix substantially. Therefore, it is technically inappropriate to refer to one as "d (z^2)" and another as "d$(x^2 - y^2)$"; however, we do so for simplicity. The d(z^2)-orbital is designated as the orbital that is most dominated by σ-antibonding interactions along the z-axis, the Mn−oxo vector, and the d$(x^2 - y^2)$ is designated as the orbital that is most dominated by σ-antibonding interactions in the xy plane. The σ bonding d$(x^2 - y^2)$ is typically dominated by contribution from the *cis*-hydroxide ligand, as it is the strongest σ-donor of the equatorial ligands.

The triplet active space of $\mathbf{1}_a$ is shown in Figure 7, and is distinctly different from the singlet. The π-bond in the π_{xz}-space

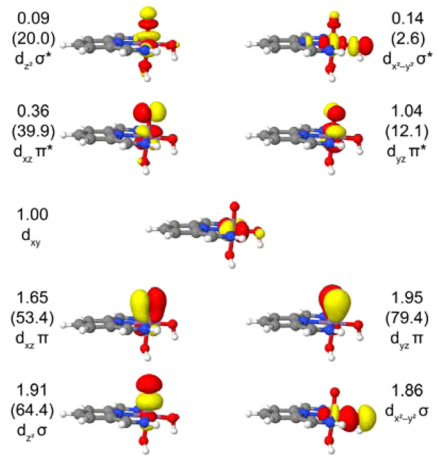

Figure 7. Natural orbitals (iso values: 0.05 a.u.) and NOONs for the triplet state of $\mathbf{1}_a$. The percentage of oxygen character of each MO is listed in parentheses.

is now considerably more covalent, with a calculated DC value of 0.75, which is closer to 1. In contrast, the π_{yz}-space is more classical with a very small DC value of 0.15. The occupation numbers show significantly noninteger values for the π_{xz}-orbitals; 1.65 for the bonding orbital, and 0.36 for the antibonding orbital. Only small deviations from integer values are seen for the d(yz) space, indicating essentially no diradical character. The wave function is unsurprisingly more multiconfigurational than the singlet, and is again dominated by the CSF shown in Figure 2 (66.4%) with single (7.9%) and double excitations (8.6%) within the π_{xz} space making up the other dominant CSFs. The weights of the CSFs are consistent with a Mulliken spin on the oxo of −0.22. While this is significant diradical character, it is not as large as what might be expected for a molecule that is best described as Mn^{IV}−$O^{\bullet}$. When comparing the extent of diradical character with the singlet case, as noted previously, there is some modest diradical character in each π bond for the singlet, whereas, for the triplet, it is almost entirely localized in the π_{xz} space. However, the sum of the diradical characters in both π-bonds is surprisingly similar for each spin state: 32% for the singlet and 40% for the triplet. This further underscores the relatively intermediate value of the diradical character in the triplet case, and, based on the

DOI: 10.1021/acscatal.6b01793
ACS Catal. 2016, 6, 7202−7216

summed diradical character, if the singlet is considered a good example of a Mn^{V}=O, then the triplet state bears significant Mn^{V}=O character, or vice versa. This would suggest that the total diradical character is not responsible for the differences in reactivity between the singlet and triplet states. This also highlights another key feature of the triplet state, which is that the radical character is directionally localized in the *xz* space, as opposed to being spherically smeared out.

Analyzing multiconfigurational wave functions is more challenging and ambiguous than their single configurational counterparts, which might lead one to wonder if the increased covalency in the π_{xz} space is simply an artifact of a multiconfigurational method/projection. In addition, it would be useful to have an unambiguous diradical to compare with the triplet. For these reasons, we examined the quintet state of **1**. As expected, the quintet electronic structure was the high-spin version of the right-most resonance structure depicted in Figure 1, where there is one α electron in a π-bonding orbital and one α electron in a π-antibonding orbital, as indicated by both the Mulliken spin and the NOONs (Figure 8). The quintet is the

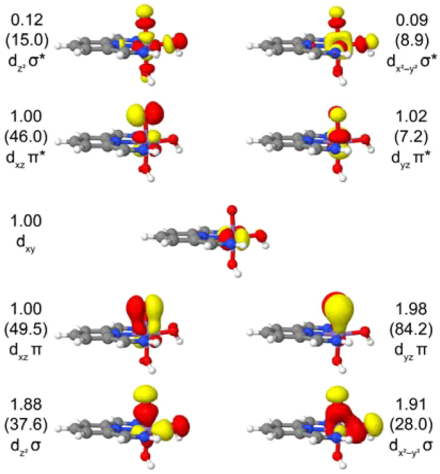

Figure 8. Natural orbitals (iso values: 0.05 a.u.) and occupation numbers for quintet $\mathbf{1}_a$. The percentage of oxygen character of each MO is listed in parentheses.

most single-configurational of the spin states analyzed, with a dominant configuration of 87%. The orbital picture from the CASSCF calculation is very similar to the triplet state, with a significantly covalent π_{xz} space and significantly polar π_{yz} space. The π_{xz} is even more covalent in the quintet state, in agreement with its larger diradical character.

The question still remains: Does the triplet have a more electron-deficient O atom than the singlet, thereby indicating that a change in physical oxidation state has occurred? A simplistic analysis would note the larger occupation number of the π_{xz}* and the lower occupation number of its bonding component, compared to the singlet case, as being indicative of charge transfer. However, the composition of these orbitals must be taken into account. In the triplet case, the π_{xz} bond is exceedingly covalent and excitations from the bonding MO into the antibonding MO have much less charge-transfer character than expected for the classical or inverted case. Thus, for a highly covalent case, even if the diradical character of the Mn−O bond were to become extremely large, it still would not have a large effect on the LMCT, as discussed with Figure 5 earlier. This exact scenario is demonstrated by comparing the EEC_{xz} for the quintet and triplet. Even though the quintet is a perfect diradical and has large spin density on oxygen, and the triplet has intermediate diradical character and much smaller spin density on oxygen (Mulliken spin of 1.0 and −0.22, respectively), the EEC_{xz} is not vastly different for the two spin states (0.96 and 1.02). There is a small decrease in electron density in the quintet oxygen, but even this is partly due to the increased covalency of the bond. These examples show how a simplistic analysis of just the diradical character, be it through NOONs, weights of CSFs, Mulliken spin, etc., is not enough to understand charge transfer, which is directly related to the physical oxidation state.

Perhaps a more important observation is that the EEC_{xz} values of 1.02 and 0.96, for the triplet and quintet, respectively, are a sizable reduction from the EEC_{xz} value of 1.25 in the singlet case. There has been significant charge transfer from the oxygen to the metal, which does not arise solely from the diradical character, but originates also from the increased covalency of the bond. Transferring electrons through a bond, as opposed to an antiferromagnetically (AF) coupled diradical, is an important distinction, and this has been discussed in detail for M(bpy) systems[80] and copper corroles.[20] The present study helps highlight the differences between these methods of electron transfer: large diradical character is expected to be correlated with charge transfer from one atom to another, but substantially less diradical character is not necessarily indicative of a lack of electron transfer, because extensive covalency between the ligand and the metal can accomplish the same task, as seen for the triplet. Comparing the singlet EEC_{xz} to the quintet, 0.29 electrons have been transferred from the oxygen to the metal, while the triplet has transferred 0.23 electrons. This is 80% of the LMCT for the quintet, despite only increasing the diradical character in the *xz*-space by ∼20% from the singlet. In terms of LMCT, the triplet can still strongly resemble the quintet, despite having much less radical character, which is an important feature for understanding the electrophilicity of the triplet state and its relationship with radical character: Relatively modest or small diradical character and spin density on oxygen can still be associated with significant LMCT and, hence, enhanced electrophilicity.

Analysis of the Mulliken charge shows that (i) singlet **1** has a charge of −0.11 on oxygen, and (ii) the triplet has a *more negative* charge of −0.23, similar to what Groves had reported earlier.[53] An increase in negative charge suggests that the triplet possesses the more-electron-rich O atom. How can this be reconciled with the electron-deficient π_{xz} space? The answer lies in the π_{yz} space. As mentioned earlier, the π_{xz} bond is very covalent, but the π_{yz} bond has become polar and classical, much more classical than the π-bonds in the singlet case. A direct comparison of the EECs for the π_{xz} and π_{yz} for both spin states show that, while the π_{xz} space is more electron-deficient for the triplet, the π_{yz} space is now much more electron-rich, making the O atom more electron-rich overall (see Table 3). A very similar situation is seen with the quintet case. Table 3 shows that the results for $\mathbf{1}_b$ and **2** exhibited the same trends. Going from the singlet to higher spin states, the O atom does not become more electron-deficient; therefore, the physical oxidation state of oxygen and Mn do not change in the manner predicted by the formal oxidation state change. There is a minor amount of electron transfer in the *z*-space on going from the singlet to the higher spin states. For example, the EEC_z of 1.33 for singlet **1** and 1.25 for triplet $\mathbf{1}_a$. However,

DOI: 10.1021/acscatal.6b01793
ACS Catal. 2016, 6, 7202−7216

Table 3. EEC Components for the (10,9) Active Space (AS) of 1 and 2 and Mulliken Charges

					Mulliken Charge	
compound	spin state	EEC_{xz}	EEC_{yz}	EEC_z	Mn	O
1	singlet	1.24	1.21	1.33[b]	1.02	−0.11
$\mathbf{1}_a$	triplet	1.02	1.68	1.25	1.11	−0.23
$\mathbf{1}_a$	quintet	0.96	1.74	1.27[b]	1.14	−0.25
$\mathbf{1}_b$	triplet	1.58	1.00	1.28[b]	1.10	−0.26
$\mathbf{1}_b$	quintet	1.61	0.96	1.25[b]	1.13	−0.34
2	singlet	1.23	1.20	1.26	1.11	−0.09
	triplet	0.98	1.69[a]	1.19	1.21	−0.21

[a]In this case, the $\pi(xz)$-orbital mixes with the $d(x^2 - y^2)$ σ-orbital. Both orbitals must be included to accurately calculate EEC_{xz}. [b]Because of deviations from perfect octahedral geometry, there is mixing between the $d(z^2)$ and $d(x^2 - y^2)$ spaces for these structures. Both spaces must be included to accurately calculate "EEC_z".

changes in the z-space are dramatically smaller than changes in the π-space.

In terms of the relative physical oxidation states, it is not appropriate to refer to the triplet/quintet case as $Mn^{IV}-O^{\bullet}$ and the singlet case as $Mn^{V}{=}O$. These relative formal oxidation state assignments are not a physically realistic way to represent the relative electron densities of the oxo ligand in these species. The key observation from our analysis is that the electron density has been *redistributed* in the high-spin cases: transferring significant electron density to the metal in one π-space, and transferring significant electron density away from the metal in an orthogonal π-space. The redistributed electron density now has an electron-poor channel where nucleophiles can approach and electron-donating groups can favorably interact. There is also now an electron-rich channel where electrophiles and electron-poor groups, such as hydrogen bonds, can favorably interact. By possessing both of these channels, the $Mn^{V}{=}O$ bond can be considered bifunctionally activated and act as a stronger Lewis acid and stronger Lewis base at the same time in orthogonal directions. Both of these features are important for metal oxo systems, and can often be exploited in analogous systems, as demonstrated recently by Ison.[81]

Interestingly, we found that the electron-deficient channel does not require dramatically large diradical character to be electrophilic. Finally, the physical oxidation states of the O atoms for the triplet and quintet are similar to each other, and actually are more reduced than for the singlet. This is an important and counterintuitive result that must be kept in mind for our assignment of physical oxidation states in redox noninnocent systems in general, not just metal oxos. The electronic redistribution in the Mn systems studied here has a similar end result to the redistribution of electron density found by Kim[75] that occurs in $Fe^{IV}{=}O$ as it converts to $Fe^{III}-O^{\bullet}$, as described earlier. However, because of the different structures and orbitals involved, the mechanism of this charge redistribution for $Fe^{IV}{=}O$ is likely different.

The Effect of Radical Character on O−O Bond Formation. The electronic structure analysis presented above suggests that (i) the relationship between electrophilicity, spin state, and oxyl radical character is nuanced, and (ii) modest amounts of radical character, compared to the unreactive singlet state, can still correspond to increased reactivity. In the literature, radical character has been proposed to be required for C−H activation and O−O bond formation. The fact that modest spin density on oxygen is present in our results suggests that the reactivity of $Mn^{V}{=}O$ complexes either is not directly dependent on the spin density at the reactant state, or only a small amount of spin density is necessary for reactivity. The former is a rather compelling idea that has been suggested by Mayer, where it is proposed that the critical feature in C−H activation by metal oxo species is not spin density/radical character but rather a strong thermodynamic driving force.[34] DFT studies on C−H activation by porphyrinoid $Mn^{V}{=}O$ using both pure and hybrid functionals have reached similar conclusions about the triplet state being able to mediate C−H activation, despite the fact that different functionals give qualitatively different electronic structures.[55,56] Pierloot has suggested that the different π-spaces can act as alternate channels for different types of radical chemistry, possibly explaining how reactivity can still be computationally observed, even with different qualitative electronic structures.[23] Similarly, McGrady and co-workers found that sulfide oxidation by triplet $Mn^{V}{=}O$ species was feasible whether mediated by the oxyl radical or the oxo, although some differences in the mechanisms were observed.[21] Given that our most-thorough analysis was for **1**, which is a model for water oxidation systems, we decided to explore the effect of functional dependence and radical character on barrier heights for O−O bond-forming reactions.

Scheme 1 shows the two archetypal mechanisms for O−O bond formation: nucleophilic attack of water on an electrophilic

Scheme 1. Typical O−O Bond Formation Mechanisms

[a]Note that, for nucleophilic attack, a Brønsted base is required to deprotonate the attacking water.

oxo and radical coupling between two oxyl radicals. **1** is capable of acting as an excellent model for both reactions, and optimized transition-state structures for each pathway are shown in Figure 9 and are discussed in detail later. For $\mathbf{1}_a$, the *cis*-hydroxo can act as a base to facilitate nucleophilic attack, whereas radical coupling can occur from a dimeric hydrogen-bonded intermediate formed between two units of $\mathbf{1}_a$. While these hydrogen-bonding interactions in the dimer do not necessarily correspond to physically relevant interactions for known water oxidation complexes or the OEC, they help to properly orient our model complex for radical coupling. As stated earlier, the alternate conformer $\mathbf{1}_b$ is still the lowest-energy structure, and is used as our reference state. Before exploring the dependence of these mechanisms on the density functional chosen, we first analyze the qualitative mechanistic features for both pathways that are mostly independent of the density functional. Here, they are reported at the B3LYP level of theory.

For radical coupling, the first step is the formation of a dimeric hydrogen-bonded adduct, denoted as **3** and similar in structure to the transition state shown in Figure 9. While electronically and entropically dimerization is not favorable, the dimer is significantly stabilized by solvation energy in water to yield an overall $\Delta G(sol)$ value for dimerization of 7.6 kcal/mol, making the dimer an accessible intermediate. The triplet

DOI: 10.1021/acscatal.6b01793
ACS Catal. 2016, 6, 7202−7216

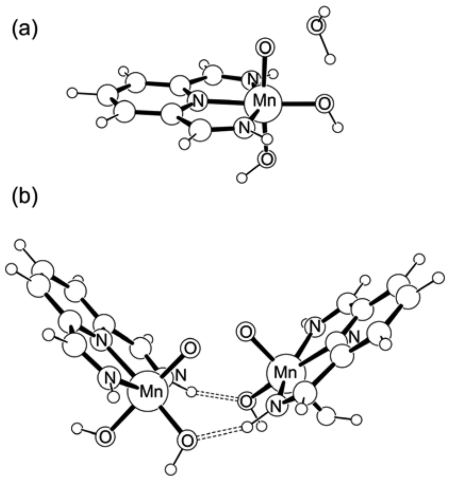

Figure 9. B3LYP-optimized O−O bond formation transition-state structures for (a) nucleophilic attack and (b) radical coupling pathways. These structures correspond to the "low spin" states as discussed in the text.

Mn^{V}=O centers can couple in a ferromagnetic fashion to yield a quintet or the spins around the two metal centers can align in an antiferromagnetic way to yield an open-shell singlet. Our calculations show that these two states are essentially isoenergetic, with the open-shell singlet being ∼1 kcal/mol higher in energy. The small magnitude of this energy difference is expected for a weakly coupled system. Because AF coupling between the two oxyl radicals is required for a smooth, spin-allowed O−O bond formation, we focused on the AF-coupled state that had a slightly higher energy. Both Mn^{V}=O units of **3** resemble a Mn^{IV}−$O^{\bullet}$, but the radical character decreases as the percentage of HF exchange is reduced, similar to what was seen for **1**. From the AF-coupled intermediate, a radical coupling transition state was only 4.8 kcal/mol higher in solution-phase free energy than **3**, leading to a calculated barrier of 12.5 kcal/mol, suggesting that radical coupling is a reasonable pathway at room temperature.

The nucleophilic attack pathway does not require any intermediates prior to O−O bond formation. A water molecule can directly attack the oxo unit while the *cis*-hydroxo acts as a Brønsted base by accepting a proton to form a hydroperoxo/aquo species. The triplet was found to be the lowest energy state for both the oxo intermediate and the transition state; however, upon formation of the Mn^{III}−OOH species, the quintet state becomes preferred as expected for a d^4 octahedral complex with weak field ligands surrounding the Mn-center. The solution-phase free energy of activation is 33.6 kcal/mol, indicating that the nucleophilic attack pathway will likely not be viable at room temperature for **1**, and it certainly is not preferred over the much more facile radical coupling pathway. This conclusion is reached no matter which DFT functional is employed. Given that we wish to quantify how much our conclusions depend on the DFT functionals, it is important to understand which energy terms are leading to the large barrier for nucleophilic attack, as detailed in Table 4. Although, for nucleophilic attack, there is a significant entropy penalty of 11.1 kcal/mol that is due to the addition of water, there is also a 13.1 kcal/mol entropic penalty for the dimerization, which is factored into the overall barrier for radical coupling. The larger penalty for nucleophilic attack is largely connected to the fact that its transition state experiences less solvation energy with a calculated $\Delta\Delta G_{solv}$ of 8.8 kcal/mol, compared to the dramatic solvent stabilization of −25.9 kcal/mol that occurs during dimerization. Electronically, the barrier is 12.8 kcal/mol, which, although sizably larger than the electronic barrier of 3.2 for the microscopic O−O radical coupling step, is still reasonable. Thus, radical coupling will undoubtedly be preferred for O−O bond formation and changes in solvation energy are clearly a critical factor in deciding the optimal reaction path.

Ideally, we wish to estimate how large of an effect radical character has on our calculated barrier heights. Fortunately, the problematic DFT functional dependence of diradical character can be exploited to study the effect of oxyl radical character on reactivity. A straightforward approach would be to characterize the two reactions with a range of HF exchange and observe the effect on O−O bond formation barrier heights. If the barriers significantly increase as the radical character diminishes, it could indicate that the radical character plays an important role in facilitating the reaction. We will refer to such an effect as *radical dependence*. Unfortunately, changing the DFT method will not solely tune the radical character, but can affect many calculated properties of the system. Most notably, it is well-known that calculated barrier heights are intrinsically functional-dependent,[82,83] regardless of whether the electronic structure is functional-dependent; we will refer to this as *intrinsic dependence*. Pure DFT is known for underestimating barrier heights, but increasing admixtures of HF exchange can partially correct for this by yielding increased barriers.[82,84] Hence, increasing the HF exchange may make the absolute barrier height larger, even though the increased oxyl radical character is making the reaction easier, depending on which effect is larger. Both of these effects must be taken into account as closely as possible. One way to approach this problem is to compare the functional dependence of the AF-coupled low spin (LS) case to that of the F-coupled high spin (HS) case (see Scheme 2). Here, this coupling is specifically referring to the interaction between Mn and the oxo oxygen. The LS (triplet) Mn^{IV}−$O^{\bullet}$ dramatically changes its electronic structure as a function of the %HF exchange, while the HS (quintet) Mn^{IV}−$O^{\bullet}$ does not. The quintet state shows some functional dependence on Mn−O bond length (see the Supporting Information) but no significant changes in oxyl radical character. Therefore, any functional dependence on reactivity for these HS cases will be largely unrelated to the radical dependence of the AF-coupled cases, and they will act essentially as a control. If the radical

Table 4. Calculated Thermodynamic Parameters with B3LYP for Reactions Important for O−O Bond Formation

reaction	ΔE (kcal/mol)	ΔZPE (kcal/mol)	$-T\Delta S$ (kcal/mol)	$\Delta\Delta G_{solv}$ (kcal/mol)	ΔG(sol) (kcal/mol)
dimerization of $^{3}\mathbf{1}_{b}$ to $^{1}\mathbf{3}$	20.34	0.15	13.10	−25.94	7.65
RC of $^{1}\mathbf{3}$ (TS)	3.18	−0.05	2.32	−0.63	4.83
NA of $^{3}\mathbf{1}_{b}$ (TS)	12.78	0.88	11.08	8.84	33.58

[a]For entries marked as "(TS)", the listed values correspond to activation parameters (i.e., $\Delta E^{\ddagger}$, as opposed to simply ΔE). All values are reported in kcal/mol, using the reference points indicated in the table.

DOI: 10.1021/acscatal.6b01793
ACS Catal. 2016, 6, 7202−7216

Scheme 2. (a) Number and Alignment of Unpaired Electrons on the Mn and O Centers for the LS and HS Nucleophilic Attack and (b) Radical Coupling Pathways

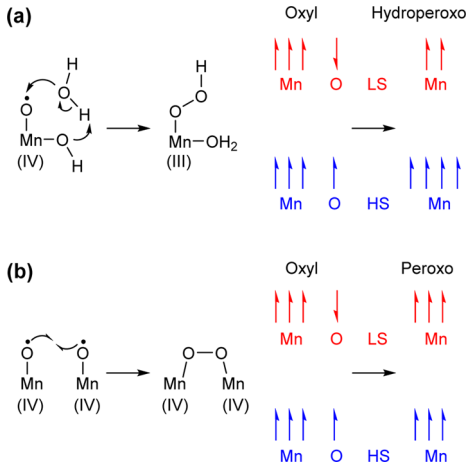

[a]The oxo moiety is always depicted as $Mn^{IV}-O\bullet$. For both the LS and HS radical coupling pathways, the $Mn^{IV}-O\bullet$ units are AF-coupled to each other (only one is shown), yielding an open-shell singlet.

dependence is significant, then the overall functional dependence of the LS reactions will be very different from the overall functional dependence of the HS reactions. By comparing the behavior of the LS and HS barrier heights, it will be possible to infer when and how much radical character starts to affect the barrier.

The electronic component of the barrier heights ($\Delta E^{\ddagger}$) for nucleophilic attack on the low-spin triplet and high-spin quintet surfaces are compared to those for the radical coupling reaction in Figure 10. While only one conformation is meaningful for the nucleophilic attack transition states, since the two hydroxides must be arranged in *anti* disposition to the oxo, the orientation of the hydroxyl group gives two slightly different conformers: $\mathbf{1}_a$ and $\mathbf{1}_b$. All barrier heights presented are relative to $\mathbf{1}_b$, and additional data in reference to $\mathbf{1}_a$ is discussed in detail in the Supporting Information.

We will first consider the nucleophilic attack data. Generally, for both LS and HS, as the amount of HF exchange is decreased, the calculated $\Delta E^{\ddagger}$ gets smaller, reflecting the intrinsic dependence described earlier. At the higher values of HF exchange, both LS and HS barriers are similar in absolute value and their DFT dependence. However, at the lower amounts of HF exchange (<5%), the LS curve starts to stabilize while the HS curve continues to decrease, which indicates that the LS reaction is now beginning to experience significant radical dependence, because of decreased oxyl radical character.

The differences between the DFT behavior for nucleophilic attack and radical coupling are immediately noticeable. For radical coupling again with large amounts of HF exchange, the calculated $\Delta E^{\ddagger}$ again decreases as the HF exchange is decreased. LS and HS decrease similarly, just as with nucleophilic attack, but they begin to diverge much more quickly. For nucleophilic attack, the LS curve began to stabilize at ~5%, but the stabilization has already started to occur for radical coupling at 15%. In fact, the radical coupling barrier heights starts to increase at <15% HF exchange, while the HS barriers continue to decrease. Because of this continuous decrease for the HS pathway, we were unable to characterize

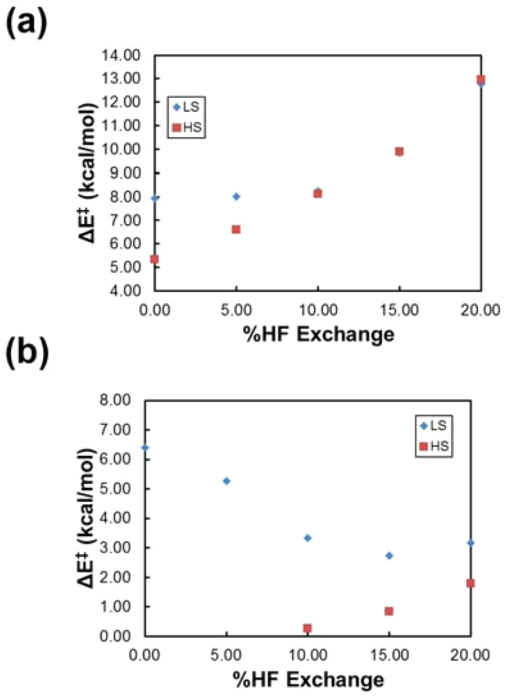

Figure 10. Dependence of electronic activation energy on HF exchange for (a) nucleophilic attack using $\mathbf{1}_b$ as a reference and (b) radical coupling. LS and HS reactions are shown as blue diamonds and red squares, respectively.

the HS radical coupling barriers with <10% HF exchange, most likely because these reactions become barrierless.

To more quantitatively assess the radical character of the oxo group while accounting for the intrinsic dependence of the energies on the different density functionals, we can examine $\Delta\Delta E^{\ddagger}$, the difference between $\Delta E^{\ddagger}_{LS}$ and $\Delta E^{\ddagger}_{HS}$, and study it as a function of the amount of HF exchange. All calculated values of $\Delta\Delta E^{\ddagger}$ for each DFT method are taken in reference to $\Delta\Delta E^{\ddagger}$ for B3LYP. Figure 11, as well as Table S4 in the Supporting

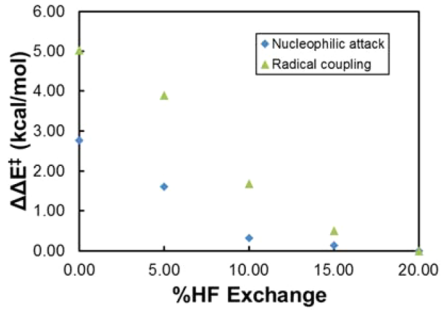

Figure 11. Difference in $\Delta E^{\ddagger}$ between LS and HS pathways for O−O bond-forming mechanisms investigated. Nucleophilic attack referenced from $\mathbf{1}_b$ is shown with blue diamonds, and radical coupling of **3** is shown as green triangles. Values are reported relative to the 20% value, for the sake of clarity.

Information, shows similar results to what was qualitatively described earlier, but a few details are more apparent: Nucleophilic attack only shows significant radical dependence at <10% for $\mathbf{1}_b$. Not surprisingly, the computed energies for the radical coupling pathways are more sensitive to which DFT functional is used than the nucleophilic attack pathway. As illustrated in Figure 11, $\Delta\Delta E^{\ddagger}$ for the radical coupling pathway

DOI: 10.1021/acscatal.6b01793
ACS Catal. 2016, 6, 7202−7216

increases as the percentage of the HF exchange is decreased. When the HF exchange is >10%, the $\Delta\Delta E^{\ddagger}$ for radical coupling is <2 kcal/mol, which is still larger than the $\Delta\Delta E^{\ddagger}$ value for nucleophilic attack, which is shown in Figure 11. In other words, for either radical coupling or nucleophilic attack, the extent of radical character in the reactant state does not have a significant effect on the barrier height once a small amount of radical character has been accrued. For nucleophilic attack, the effect of going from B3LYP to B3LYP[0] is 2.77 kcal/mol. While this is a non-negligible effect on a barrier height, it is not large enough to indicate that radical character in the reactant state is a required condition for facile nucleophilic attack. This qualitatively agrees with the observation from our CASSCF results earlier that only a modest amount of diradical character needs be associated with a significantly electrophilic π-space. Generally, such an effect may artificially appear from just analyzing the total spin if the β spin in the *xz*-space was being cancelled out by a large amount of α spin in the *yz*-space. However, as shown earlier, the amount of α spin is generally quite small (~0.2), a result which is also cleanly shown in Pierloot's work;[23] hence, the changes in β spin are much more dramatic. In addition, recall that the explicit diradical character in the *xz*-space varies as a function of %HF exchange, similar to the total spin. Hence, Figures 11 and 12 can just as easily be interpreted in terms of the change in diradical character in the *xz*-space as they are in terms of the Mulliken spin.

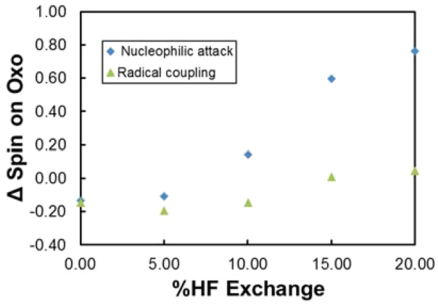

Figure 12. Changes in Mulliken spin on the oxo oxygen at the O−O bond forming TS. Data are shown for nucleophilic attack from $\mathbf{1}_b$ (blue diamonds) and radical coupling from **3** (green triangles).

For radical coupling, the effect of going from B3LYP to B3LYP[0] is larger at 5.03 kcal/mol, so it will be a more important factor for dictating reactivity. Adding these amounts of energy to the B3LYP calculated barriers for nucleophilic attack or radical coupling has no effect on any of the general conclusions reached, underscoring that the absolute magnitude of radical character may not be the most critical feature for understanding these barrier heights. The fact that radical coupling should be more sensitive to radical character than nucleophilic attack agrees well with chemical intuition, given that the radical coupling mechanism inherently involves spin coupling. These differences in the magnitude of radical dependence may also be related to the fact that there are two oxyl radical units being affected by the change in radical character for radical coupling, whereas for nucleophilic attack, only one is being perturbed. Regardless, for either of these reasons we would expect radical coupling to be more dependent on radical character than nucleophilic attack, and our calculations confirm this expectation.

Although the radical character of the oxo group in the reactant structures are important and have been the focus of many studies, including this our own work, it is also important to understand its role in the transition states. Figure 12, as well as Table S5 in the Supporting Information, depict how the Mulliken spin on the oxo evolves going from the reactant to the transition state on the low-spin manifold traversing the radical coupling and nucleophilic attack pathways. For the radical coupling path, the spin density of the oxo oxygen in the transition state is similar to that of the reactant (within 0.2) and usually shows slightly larger radical character. For nucleophilic attack, the oxo spin in the TS is always very close to 0, ranging from 0.1 to −0.01, which means that the triplet nucleophilic attack TS only has a small amount of oxyl radical character and is relatively insensitive to the exchange-correlation functional used. Since the nucleophilic attack TS electronic structure closely resembles that of a simple LS Mn(III) hydroperoxo, it can be said that the nucleophilic attack TS is "electronically late". One possible interpretation of this data is that, because the nucleophilic attack TS has more oxyl character than the reactant only below ~10% HF exchange, having to induce oxyl radical character at the TS, instead of already being present in in the reactant, may contribute to the radical dependence. A similar effect may occur for radical coupling. In examining barrier heights for Fe^{IV}═O-mediated HAT, the "preparation energy" involved in forming an oxyl radical was shown to be a substantial component of the barrier by Kim,[75] although, in this work, it would appear to be less significant.

Sorting out the many ways that exchange-correlation functionals can influence calculated energetics is difficult, but our calculations suggest that the nucleophilic attack pathway is well-captured in DFT. Additional discussion of potential complicating factors and how they affect a similar analysis with the Minnesota functionals is provided in the Supporting Information. The DFT results show that, while the oxyl radical character of the reactant will impact the barrier height, the effects are modest. For either pathway, the oxyl radical character has its largest effect on the barrier height only when the radical character is very small. In other words, a small amount of oxyl radical character is basically as effective as a large amount. This gives comforting agreement with the CASSCF-determined electronic structure, which showed only a modest amount of oxyl radical character. The fact that the CASSCF radical character/spin density is smaller than the B3LYP-predicted results should not have a significant impact on reactivity. This may be related to the fact that, even with a modest amount of diradical character, the triplet state already has a substantially electrophilic *xz*-space, despite the O atom being more electron-rich overall in the *yz*-space. Clearly, the relationship between the electrophilicity of an atom, its radical character, and the physical oxidation state is not always straightforward. Generally, it is important to consistently gauge when these radical effects will be important, as it is expected that other reactions may show similarly weak dependencies on radical character, as seen for nucleophilic attack.

CONCLUSIONS

Clarifying the numerous ambiguities surrounding the electronic structure of Mn^{V}═O complexes is invariably necessary for understanding and predicting how nature uses this functional group, as well as for designing better catalysts. The severe functional dependence of BS-DFT makes it exceedingly difficult to quantify the degree of diradical character, spin density, or Mn−O bond lengths. CASSCF and NEVPT2 calculations for our six-coordinate systems corroborated recent results that the

DOI: 10.1021/acscatal.6b01793
ACS Catal. 2016, 6, 7202−7216

diradical character of pseudo-octahedral Mn^{V}=O is modest but significant and is best characterized as intermediate and lying between the two extremes often presented in the literature. Perhaps the more important findings were what the calculations exposed about the relationship between spin density and the physical oxidation state. Because the diradical pair was confined to a particularly covalent bond, the extent of diradical character had only a modest effect on charge transfer from the oxygen to the Mn-center. Charge transfer was still significant, but it was not arising solely from diradical character, but also the covalency of the bond. Therefore, while extensive diradical character is most likely a good indication of charge transfer, it is not a necessary condition. Furthermore, even though there was significant charge transfer from the oxygen to the metal in one π-space, there was a compensatory charge transfer from the metal to the oxygen in the other π-space, showing that the oxo oxygen for the high-spin oxyls are actually slightly more electron-rich than the low-spin oxos. This also suggests that the Mn^{V}=O bond simultaneously contains both Lewis acidic and Lewis basic functionality, which is a conclusion that can only be understood by appreciating the actual changes in the physical oxidation state. Finally, the functional dependence of the oxyl radical character was used to estimate how significant oxyl radical character is for the O−O bond formation kinetics. It was found that the effect of radical character was relatively small for nucleophilic attack, and likely not a required feature for this mechanism; however, the oxyl radical effect was more sizable for radical coupling pathways. For both mechanisms, however, these effects were not particularly significant once a small amount of radical character had been built up in the reactant, showing that the CASSCF results reported here do not imply diminished reactivity.

■ ASSOCIATED CONTENT

Supporting Information

The Supporting Information is available free of charge on the ACS Publications website at DOI: 10.1021/acscatal.6b01793.

Computational details, cartesian coordinates, vibrational frequencies, energies of all calculated structures, and additional discussion (PDF)

■ AUTHOR INFORMATION

Corresponding Author

*E-mail: mbaik2805@kaist.ac.kr.

Notes

The authors declare no competing financial interest.

■ ACKNOWLEDGMENTS

We thank the Research Corporation (Scialog Award to M.-H.B.) and the Institute for Basic Science (No. IBS-R10-D1) in Korea for financial support.

■ REFERENCES

(1) Yang, X.; Baik, M.-H. *J. Am. Chem. Soc.* **2006**, *128*, 7476−7485.
(2) Sproviero, E. M.; Gascón, J. A.; McEvoy, J. P.; Brudvig, G. W.; Batista, V. S. *J. Am. Chem. Soc.* **2008**, *130*, 3428−3442.
(3) Sala, X.; Maji, S.; Bofill, R.; Garcia-Antón, J.; Escriche, L.; Llobet, A. *Acc. Chem. Res.* **2014**, *47*, 504−516.
(4) Kikuchi, T.; Tanaka, K. *Eur. J. Inorg. Chem.* **2014**, *2014*, 607−618.
(5) Fillol, J. L.; Codolà, Z.; Garcia-Bosch, I.; Gómez, L.; Pla, J. J.; Costas, M. *Nat. Chem.* **2011**, *3*, 807−813.
(6) Wasylenko, D. J.; Ganesamoorthy, C.; Borau-Garcia, J.; Berlinguette, C. P. *Chem. Commun.* **2011**, *47*, 4249−4251.
(7) Thomsen, J. M.; Sheehan, S. W.; Hashmi, S. M.; Campos, J.; Hintermair, U.; Crabtree, R. H.; Brudvig, G. W. *J. Am. Chem. Soc.* **2014**, *136*, 13826−13834.
(8) Limburg, J.; Vrettos, J. S.; Liable-Sands, L. M.; Rheingold, A. L.; Crabtree, R. H.; Brudvig, G. W. *Science* **1999**, *283*, 1524−1527.
(9) Karlsson, E. A.; Lee, B.; Akermark, T.; Johnston, E. V.; Karkas, M. D.; Sun, J.; Hansson, O.; Backvall, J.; Akermark, B. *Angew. Chem., Int. Ed.* **2011**, *50*, 11715−11718.
(10) Young, K. J.; Takase, M. K.; Brudvig, G. W. *Inorg. Chem.* **2013**, *52*, 7615−7622.
(11) Shimazaki, Y.; Nagano, T.; Takesue, H.; Ye, B.-H.; Tani, F.; Naruta, Y. *Angew. Chem., Int. Ed.* **2004**, *43*, 98−100.
(12) Gao, Y.; Liu, J. H.; Wang, M.; Na, Y.; Akermark, B.; Sun, L. *Tetrahedron* **2007**, *63*, 1987−1994.
(13) Lee, W.-T.; Muñoz, S. B., III; Dickie, D. A.; Smith, J. M. *Angew. Chem., Int. Ed.* **2014**, *53*, 9856−9859.
(14) McEvoy, J. P.; Brudvig, G. W. *Chem. Rev.* **2006**, *106*, 4455−4483.
(15) Umena, Y.; Kawakami, K.; Shen, J. R.; Kamiya, N. *Nature* **2011**, *473*, 55−60.
(16) Kok, B.; Forbush, B.; McGloin, M. *Photochem. Photobiol.* **1970**, *11*, 457−475.
(17) Lundberg, M.; Blomberg, M. R. A.; Siegbahn, P. E. M. *Inorg. Chem.* **2004**, *43*, 264−274.
(18) Cox, N.; Pantazis, D. A.; Neese, F.; Lubitz, W. *Acc. Chem. Res.* **2013**, *46*, 1588−1596.
(19) Boguslawski, K.; Jacob, C. R.; Reiher, M. *J. Chem. Theory Comput.* **2011**, *7*, 2740−2752.
(20) Pierloot, K.; Zhao, H.; Vancoillie, S. *Inorg. Chem.* **2010**, *49*, 10316−10329.
(21) Sameera, W. M. C.; McGrady, J. E. *Dalton Trans.* **2008**, 6141−6149.
(22) Herrmann, C.; Podewitz, M.; Reiher, M. *Int. J. Quantum Chem.* **2009**, *109*, 2430−2446.
(23) Venturinelli Jannuzzi, S. A.; Phung, Q. M.; Domingo, A.; Formiga, A. L. B.; Pierloot, K. *Inorg. Chem.* **2016**, *55*, 5168−5179.
(24) Prokop, K. A.; de Visser, S. P.; Goldberg, D. P. *Angew. Chem., Int. Ed.* **2010**, *49*, 5091−5095.
(25) Neu, H. M.; Baglia, R. A.; Goldberg, D. P. *Acc. Chem. Res.* **2015**, *48*, 2754−2764.
(26) Lansky, D. E.; Goldberg, D. P. *Inorg. Chem.* **2006**, *45*, 5119−5125.
(27) Kerber, W. D.; Goldberg, D. P. *J. Inorg. Biochem.* **2006**, *100*, 838−857.
(28) Hull, J. F.; Balcells, D.; Sauer, E. L. O.; Raynaud, C.; Brudvig, G. W.; Crabtree, R. H.; Eisenstein, O. *J. Am. Chem. Soc.* **2010**, *132*, 7605−7616.
(29) Balcells, D.; Moles, P.; Blakemore, J. D.; Raynaud, C.; Brudvig, G. W.; Crabtree, R. H.; Eisenstein, O. *Dalton Trans.* **2009**, 5989−6000.
(30) Balcells, D.; Raynaud, C.; Crabtree, R. H.; Eisenstein, O. *Chem. Commun.* **2008**, 744−746.
(31) Ghosh, A.; Gonzalez, E. *Isr. J. Chem.* **2000**, *40*, 1−8.
(32) Steene, E.; Wondimagegn, T.; Ghosh, A. *J. Phys. Chem. B* **2001**, *105*, 11406−11413.
(33) Sahu, S.; Goldberg, D. P. *J. Am. Chem. Soc.* **2016**, *138*, 11410−11428.
(34) Saouma, C. T.; Mayer, J. M. *Chem. Sci.* **2014**, *5*, 21−31.
(35) Neese, F. *WIREs Comput. Mol. Sci.* **2012**, *2*, 73−78.
(36) Becke, A. D. *Phys. Rev. A: At., Mol., Opt. Phys.* **1988**, *38*, 3098−3100.
(37) Becke, A. D. *J. Chem. Phys.* **1993**, *98*, 5648−5652.
(38) Vosko, S. H.; Wilk, L.; Nusair, M. *Can. J. Phys.* **1980**, *58*, 1200−1211.
(39) Lee, C.; Yang, W.; Parr, R. G. *Phys. Rev. B: Condens. Matter Mater. Phys.* **1988**, *37*, 785−789.
(40) Stephens, P. J.; Devlin, F. J.; Chabalowski, C. F.; Frisch, M. J. *J. Phys. Chem.* **1994**, *98*, 11623−11627.
(41) Hariharan, P. C.; Pople, J. A. *Theor. Chim. Acta* **1973**, *28*, 213−222.

DOI: 10.1021/acscatal.6b01793
ACS Catal. 2016, 6, 7202−7216

(42) Hay, P. J.; Wadt, W. R. *J. Chem. Phys.* **1985**, *82*, 299−310.
(43) Dunning, T. H., Jr. *J. Chem. Phys.* **1989**, *90*, 1007−1023.
(44) Balabanov, N. B.; Peterson, K. A. *J. Chem. Phys.* **2005**, *123*, 064107/1−064107/15.
(45) *Jaguar, version 8.1*; Schrödinger, LLC: New York, 2013.
(46) Veryazov, V.; Malmqvist, P. Å.; Roos, B. O. *Int. J. Quantum Chem.* **2011**, *111*, 3329−3338.
(47) Pierloot, K. *Mol. Phys.* **2003**, *101*, 2083−2094.
(48) Zhao, H.; Pierloot, K.; Langner, E. H. G.; Swarts, J. C.; Conradie, J.; Ghosh, A. *Inorg. Chem.* **2012**, *51*, 4002−4006.
(49) Kim, J.; Kim, J.; Ihee, H. *J. Phys. Chem. A* **2013**, *117*, 3861−3868.
(50) Yang, T.; Quesne, M. G.; Neu, H. M.; Cantú Reinhard, F. G.; Goldberg, D. P.; de Visser, S. P. *J. Am. Chem. Soc.* **2016**, DOI: 10.1021/jacs.6b05027.
(51) Siegbahn, P. E. *Inorg. Chem.* **2008**, *47*, 1779−1786.
(52) Sameera, W. M. C.; McKenzie, C. J.; McGrady, J. E. *Dalton Trans.* **2011**, *40*, 3859−3870.
(53) De Angelis, F.; Jin, N.; Car, R.; Groves, J. T. *Inorg. Chem.* **2006**, *45*, 4268−4276.
(54) Jin, N.; Groves, J. T. *J. Am. Chem. Soc.* **1999**, *121*, 2923−2924.
(55) Balcells, D.; Raynaud, C.; Crabtree, R. H.; Eisenstein, O. *Inorg. Chem.* **2008**, *47*, 10090−10099.
(56) Janardanan, D.; Usharani, D.; Shaik, S. *Angew. Chem., Int. Ed.* **2012**, *51*, 4421−4425.
(57) Jin, N.; Ibrahim, M.; Spiro, T. G.; Groves, J. T. *J. Am. Chem. Soc.* **2007**, *129*, 12416−12417.
(58) Jin, N.; Bourassa, J. L.; Tizio, S. C.; Groves, J. T. *Angew. Chem., Int. Ed.* **2000**, *39*, 3849−3851.
(59) Note that this is not exactly the same as the pure functional BLYP, in which case "b" and "c" in eq 1 would both be set at 1.0. BLYP gives qualitative results similar to those of B3LYP[0].
(60) Reiher, M. *Inorg. Chem.* **2002**, *41*, 6928−6935.
(61) Taguchi, T.; Gupta, R.; Lassalle-Kaiser, B.; Boyce, D. W.; Yachandra, V. K.; Tolman, W. B.; Yano, J.; Hendrich, M. P.; Borovik, A. S. *J. Am. Chem. Soc.* **2012**, *134*, 1996−1999.
(62) Reiher, M.; Salomon, O.; Hess, B. A. *Theor. Chem. Acc.* **2001**, *107*, 48−55.
(63) Salomon, O.; Reiher, M.; Hess, B. A. *J. Chem. Phys.* **2002**, *117*, 4729−4737.
(64) Saito, T.; Kataoka, Y.; Nakanishi, Y.; Matsui, T.; Kitagawa, Y.; Kawakami, T.; Okumura, M.; Yamaguchi, K. *Int. J. Quantum Chem.* **2009**, *109*, 3649−3658.
(65) Chen, H.; Ikeda-Saito, M.; Shaik, S. *J. Am. Chem. Soc.* **2008**, *130*, 14778−14790.
(66) Shaik, S.; Chen, H. *J. Biol. Inorg. Chem.* **2011**, *16*, 841−855.
(67) Danovich, D.; Shaik, S.; Chen, H. In *Comprehensive Inorganic Chemistry II*, Second Edition; Poeppelmeier, K., Ed.; Elsevier: Amsterdam, 2013; pp 1−57.
(68) Isobe, H.; Soda, T.; Kitagawa, Y.; Takano, Y.; Kawakami, T.; Yoshioka, Y.; Yamaguchi, K. *Int. J. Quantum Chem.* **2001**, *85*, 34−43.
(69) Koizumi, K.; Shoji, M.; Nishiyama, Y.; Maruno, Y.; Kitagawa, Y.; Soda, K.; Yamanaka, S.; Okumura, M.; Yamaguchi, K. *Int. J. Quantum Chem.* **2004**, *100*, 943−956.
(70) Yamaguchi, K.; Shoji, M.; Saito, T.; Isobe, H.; Nishihara, S.; Koizumi, K.; Yamada, S.; Kawakami, T.; Kitagawa, Y.; Yamanaka, S.; Okumura, M. *Int. J. Quantum Chem.* **2010**, *110*, 3101−3128.
(71) Jacob, C. R.; Reiher, M. *Int. J. Quantum Chem.* **2012**, *112*, 3661−3684.
(72) Bachler, V.; Olbrich, G.; Neese, F.; Wieghardt, K. *Inorg. Chem.* **2002**, *41*, 4179−4193.
(73) Neese, F. *Coord. Chem. Rev.* **2009**, *253*, 526−563.
(74) Salem, L.; Rowland, C. *Angew. Chem., Int. Ed. Engl.* **1972**, *11*, 92−111.
(75) Mai, B. K.; Kim, Y. *Inorg. Chem.* **2016**, *55*, 3844−3852.
(76) Gebhard, M. S.; Koch, S. A.; Millar, M.; Devlin, F. J.; Stephens, P. J.; Solomon, E. I. *J. Am. Chem. Soc.* **1991**, *113*, 1640−1649.
(77) Note that a bond in and of itself cannot be considered multiconfigurational. Rather, it is a property of the entire wave function. In this context, however, we are describing the influence that certain bonds can have on inducing the multiconfigurational character of the wave function. This is generally quantified by analyzing the occupation numbers of natural orbitals assigned to a given bond.
(78) In our work, these percent compositions were the Löwdin orbital compositions of the CASSCF natural orbitals.
(79) Sears, J. S.; Sherrill, C. D. *J. Chem. Phys.* **2006**, *124*, 144314.
(80) Scarborough, C. C.; Wieghardt, K. *Inorg. Chem.* **2011**, *50*, 9773−9793.
(81) Smeltz, J. L.; Lilly, C. P.; Boyle, P. D.; Ison, E. A. *J. Am. Chem. Soc.* **2013**, *135*, 9433−9441.
(82) Zhao, Y.; González-García, N.; Truhlar, D. G. *J. Phys. Chem. A* **2005**, *109*, 2012−2018.
(83) Zhao, Y.; Truhlar, D. G. *Acc. Chem. Res.* **2008**, *41*, 157−167.
(84) Lynch, B. J.; Fast, P. L.; Harris, M.; Truhlar, D. G. *J. Phys. Chem. A* **2000**, *104*, 4811−4815.

DOI: 10.1021/acscatal.6b01793
ACS Catal. 2016, 6, 7202−7216